ELSEVIER

Scopus

doi

Journal of Vibration Engineering

ISSN:1004-4523

Registered

- SCOPUS
- GOOGLE SCHOLAR
- DIGITAL OBJECT IDENTIFIER (DOI)
- IMPACT FACTOR 6.1

Our Website
www.jove.science

Blood Flow Characteristics in a Mildly Stenosed Bifurcated Artery under Varying Darcy Numbers

G. Madhava Rao[1], Adigoppula Raju[2,*], G. Swamy Reddy[3]

[1]Department of Mathematics, Koneru Lakshmaiah Education Foundation, Bowrampet, Hyderabad-500043, Telangana, India.
[2]Department of Applied Science, Symbiosis Institute of Technology, Symbiosis International (Deemed University), Pune, India.
[3]Department of Mathematics, SR University, Warangal- 506371, Telangana, India.

Abstract:

This article addresses with the effect of the permeability constant on blood flow attributes by treating blood as a nanofluid passing through a branched artery. The branched artery contains a tiny stenosis within the primary lumen, which is surrounded by a porous medium. Division of the considered artery is believed to be symmetric about its own axis of finite length. The physical scenario is described as a mathematical model and then solved by using the Block elimination strategy executed with MATLAB. Variations in temperature, velocity, flow rate, and impedance with respect to the permeability parameter are analyzed graphically. Present findings are helpful to the doctor's fraternity to make analyses and draw conclusions about arterial diseases.

Key words:- Blood flow, Nanofluid, Bifurcated artery, Stenosis, Darcy Number.

1. Introduction:

The arterial vasculature is accountable to distribute oxygen-rich blood to the different tissues and organs from the heart. Studying blood flow patterns helps in understanding how the heart and blood vessels interact and how they respond to physiological demands. Abnormal blood flow can indicate or lead to conditions like atherosclerosis, aneurysms, hypertension, and arterial stenosis. For a healthy life cycle, maintaining a proper functionality of the heart and arterial system are crucial. However, in recent years, cardiovascular and arterial diseases have become a leading cause of mortality worldwide. A significant contributor to these diseases is the irregular and

abnormal flow of blood through arteries, often resulting from the rupture of at heromatous plaques. These plaques, when accumulated within the arterial system, obstruct blood flow and lead to stenosis, a condition that restricts blood circulation. Early-stage stenosis can often be treated; however, advanced stages involving severe plaque build-up block blood flow to critical vascular regions, potentially causing heart attacks. Numerous studies [1–6] have demonstrated the Rheometric characteristics of blood are essential for analyzing cardiovascular diseases. Furthermore, Liu and Liu [7] examined the effects of heat and mass transfer of blood flow in stenosed tapered arteries. In their work, Amos et al. [8] analyzed the repercussion of body acceleration and slip repercussions on magnetohydrodynamic pulsatile blood flow in an inclined stenosed artery.

The movement of blood in arteries is heavily influenced by the severity and morphology of stenosis. Deposition of calcium salts in vessel walls makes them stiff and narrow. Fried fast, fatty cuts of red meat, hydrogenated oils, have been identified as a critical factor in stenosis development. Heavy drinking contributes to high triglycerides, hypertension, and arterial damage. A mathematical model was designated by Karim et al. [9] to explorw blood flow in a restricted artery, it revealed that the severity of stenosis and the tapering angle contributed to increase wall shear stress and reduce velocity. Gandhi *et.al.* [10] introduced a novel MHD Casson nanofluid model to examine blood flow in a stenosed artery. This study focused on the combined influence of magnetic field and nanoparticle size on momentum diffusion and heat transfer. An advanced fractional fluid model based on ternary nanoparticles (Cu, Ag, CuO) was suggested by Shahzadi et al. [11] assess blood flow in the obliquely stenosed aneurysmal artery. The study emphasized that ternary nanoparticles display superior capability in reducing wall shear stress.

Throughout the past few decades, substantial research has been carried out to study the pulsatile behavior of blood flow in the artery with stenosis. Within the cardiovascular system, flow patterns characterized by cyclic variations in velocity and pressure originate from the rhythmic pumping action of the heart during each cardiac cycle [12–14]. Oscillatory flow dynamics are crucial to understanding key physiological processes—ranging from blood pressure regulation to nutrient and oxygen delivery—and are closely linked to arterial disorders like atherosclerosis and hypertension. For this reason, a large body of work has been devoted to exploring pulsatile blood flow and its clinical significance [12–16].

Aortic sclerosis, the early stage leading to aortic stenosis (AS), occurs in about one-third of individuals older than 65 years [17–18]. This condition commonly progresses to calcific AS [19], a long-term disorder that begins with cusp thickening and calcification without significant hemodynamic consequence but culminates in heavily calcified and immobile cusps, causing severe narrowing of the valve. Evidence increasingly indicates that the process is not solely the result of mechanical degeneration but also entails active biological mechanisms such as inflammation and lipid infiltration, closely resembling the pathophysiology of atherosclerosis [17–20].

Bifurcated arteries, such as the carotid artery, are critical areas of focus in cardiovascular research due to their susceptibility to plaque accumulation, which often leads to chronic diseases. The geometry and flow dynamics of bifurcated arteries have been studied extensively to understand their role in disease progression. [20] analyzed hemodynamic changes in bifurcated arteries with high-grade stenosis. Movement of blood through a bifurcated artery by treating blood as nano fluid has been explained in [21], [22], [23]. These studies have provided invaluable insights into the impact of branch of artery on blood flow dynamics and stenosis

progression. In the current research, the repercussion of Darcy number on blood flow characteristics has been discussed.

2. Mathematical Formulation, Materials and Method:

Transit of blood through a branched artery containing a minor stenosis in the main lumen is modeled using a steady, homogeneous, incompressible nanofluid framework, as illustrated in fig.1. Blood is assumed as copper-water nanofluid of viscosity μ_{nf} and density ρ_{nf}. Artery bifurcation is symmetric about the main axes of branched artery and it is in limited length. Curvature is taken at the starting point of the junction along the side and near the flow division so that the chance of boundary layer breakdowns (if any occurs) can be curbed. Acceleration due to gravity (g) acts in a downward orientation. Except density, all characteristics of fluid are treated to be constant.

The flow domain is described in a cylindrical polar coordinate (r, θ, z). within this framework, the governing equations for copper–water nanofluid flow are presented below

$$u_r + \frac{u}{r} + w_z = 0 \tag{1}$$

$$\rho_{nf}\left[uu_r + wu_z\right] = -p_r + \mu_{nf}\left[2u_r\right]_r + \mu_{nf}\left[2u_z + w_r\right]_z - \frac{\mu_{nf}}{K}u \tag{2}$$

$$\rho_{nf}\left[uw_r + ww_z\right] = -p_z + \mu_{nf}\left[2w_z\right]_z + \frac{\mu_{nf}}{r}\left[r\left(u_z + w_r\right)\right]_r + \rho_{nf} g\beta_2 (T - T_0) - \sigma B_0^2 w - \frac{\mu_{nf}}{K}w \tag{3}$$

$$(\rho_{cp})_{nf}\left[uT_r + wT_z\right] = K_{nf}\left[T_{rr} + \frac{1}{r}T_r + T_{zz}\right] + Q_1 \tag{4}$$

In this context, u and w correspond to the radial and longitudinal velocity components. K is the porous wall permeability and Q_1 is the heat generation term. β_2, σ and B_0 represents volumetric thermal expansion, electrical conductivity, and magnetic field strength, respectively. T is the local temperature, while μ_{nf}, ρ_{nf} $(\rho c_p)_{nf}$, and k_{nf} correspond to the nanofluid's dynamic viscosity, effective density, heat capacity and thermal conductivity, respectively.

These parameters are as follows

$$\left.\begin{aligned} &\frac{\mu_{nf}}{\mu_f}=\frac{1}{(1-\phi)^{2.5}},\ \frac{\rho_{nf}}{\rho_f}=(1-\phi)+\phi\frac{\rho_s}{\rho_f},\ \alpha_{nf}=\frac{K_{nf}}{\left(\rho c_p\right)_{nf}},\\ &\frac{\left(\rho c_p\right)_{nf}}{\left(\rho c_p\right)_f}=(1-\phi)\left(\rho c_p\right)_f+\phi\frac{\left(\rho c_p\right)_s}{\left(\rho c_p\right)_f},\ \frac{K_{nf}}{K_f}=\left[\frac{K_s+2K_f-2\phi\left(K_f-K_s\right)}{K_s+2K_f+\phi\left(K_f-K_s\right)}\right] \end{aligned}\right\} \quad (5)$$

where α_{nf} is the overall thermal diffusivity. Functional thermal conductivity given in eq. 5 does not taken the interfacial thermal resistance between fluid and nanoparticles. Moreover, it applies only to spherical particles, where size effects are significant. A more comprehensive model should account for both particle size and interface resistance. Since, copper nanoparticle thermal conductivity $K_s=401Wm^{-1}(K^{-1})$ is much greater than the water thermal conductivity $K_f=0.613Wm^{-1}(K^{-1})$, then the proportion K_f/K_s can be estimated as zero [22].

Therefore, $\frac{K_s+2K_f-2\phi\left(K_f-K_s\right)}{K_s+2K_f+\phi\left(K_f-K_s\right)}=1+3\phi$.

Bifurcated artery is described geometrically by the functions $R_1(z)$ and $R_2(z)$, representing outer and inner arterial walls, respectively [24] as,

$$R_1(z)=\begin{cases} a, & 0\le z\le d' \quad and \quad d'+l_0\le z\le z_1\\ (a-\frac{4\grave{o}}{l_0^2}(l_0(z-d')-(z-d')^2), & d'\le z\le d'+l_0\\ (a+r_0-\sqrt{r_0^2-(z-z_1)^2}), & z_1\le z\le z_2\\ (2r_1sec\beta+(z-z_2)tan\beta), & z_2\le z\le z_{max} \end{cases}$$

$$R_2(z)=\begin{cases} 0, & 0\le z\le z_3\\ \sqrt{(r_0^{'})^2-(z-z_3-r_0^{'})^2}, & z_3\le z\le z_3+r_0^{'}(1-sin\beta)\\ (r_0^{'}cos\beta+z_4), & z_3+r_0^{'}(1-sin\beta)\le z\le z_{max} \end{cases}$$

the region unaffected by stenosis; r_1 corresponds to the daughter artery radius. The lateral junction and apex exhibit radii of curvature r_0 and r_0', respectively. The stenosis spans a length l_0, initiating at a position d′ along the axial direction. Locations z_1, z_2, and z_3 define the inlet, lateral junction and apex. The half-angle of the bifurcation is visualized by β, and ε denotes the peak stenosis height, occurring at the midpoint $z = d' + l_0/2$. Total length of the bifurcated arterial structure is given by z_{max}.

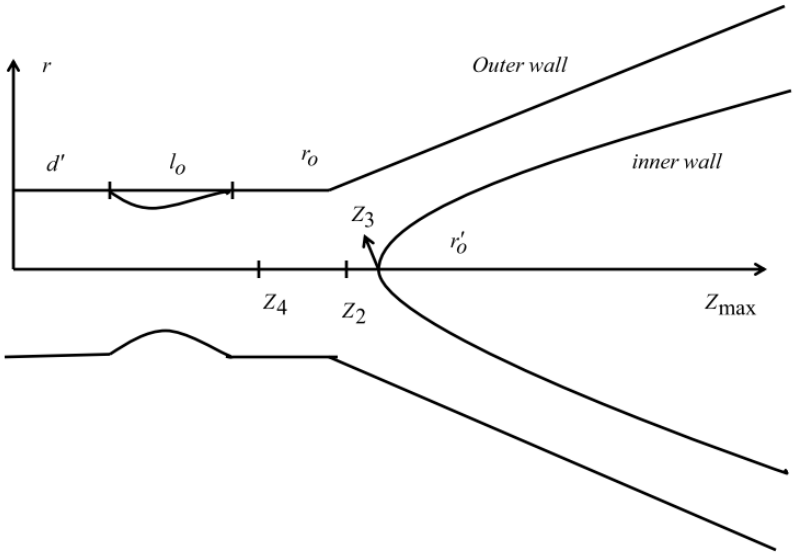

Figure-1. Schematic representation of bifurcated artery stenosis

The physical problem is constrained by the following boundary conditions

$$\left.\begin{array}{llll} w_r = 0, & T_r = 0, & \text{on} \quad r = 0 & \text{for} \quad 0 \le z \le z_3 \\ w = 0, & T = T_0, & \text{on} \quad r = R_1(z) & \text{for all } z \\ w = 0, & T_r = 0, & \text{on} \quad r = R_2(z) & \text{for } z_3 \le z \le z_{max} \end{array}\right\} \tag{6}$$

Let L, w_0, and T_w represent the characteristic length, velocity, and outer wall temperature of the artery, respectively. Using, the following non - dimensionalization scheme.

$$\left.\begin{aligned} &r = a\,\tilde{r},\ u = \frac{aw_0\tilde{u}}{L},\ z = L\,\tilde{z},\ w = w_0\,\tilde{w},\ d = L\,\tilde{d},\ p = \frac{Lw_0\mu_f\,\tilde{p}}{a^2},\\ &\Theta = \frac{T-T_0}{T_w-T_0},\ R_1(z) = a\,\tilde{R}_1(\tilde{z}),\ R_2(z) = a\,\tilde{R}_2(\tilde{z}),\ r_1 = a\,\tilde{r}_1,\ z_1 = a\,\tilde{z}_1, \end{aligned}\right\} \tag{7}$$

Equations (1) - (4) under low Reynolds number flow case, after dropping tildes,

$$p_r = 0 \tag{8}$$

$$-p_z + \frac{1}{(1-\phi)^{2.5}}\left[w_{rr} + \frac{1}{r}w_r\right] - \left(\frac{1}{D_a} + H^2\right)w + G_r\Theta = 0 \tag{9}$$

$$\Theta_{rr} + \frac{1}{r}\Theta_r + s\left(1+3\phi\right) = 0 \tag{10}$$

where $G_r = \dfrac{g\beta_2 a^2(T_w - T_0)\rho_{nf}}{w_o\mu_f}$ Grashof number, $D_a = \dfrac{K}{L^2}$ Darcy number, $H = B_0 a\sqrt{\dfrac{\sigma}{\mu_f}}$ Hartmann number, $s = \dfrac{Q_1 a^2}{k_f(T_w - T_0)}$ Heat source parameter.

Subject to the associated non-dimensional boundary conditions are

$$\left.\begin{aligned} &w_r = 0,\quad \Theta_r = 0,\quad \text{on}\quad r = 0\quad \text{for}\quad 0 \le z \le z_3\\ &w = 0,\quad \Theta = 0,\quad \text{on}\quad r = R_1(z)\quad \text{for all}\ \ z\\ &w = 0,\quad \Theta_r = 0,\quad \text{on}\quad r = R_2(z)\quad \text{for}\quad z_3 \le z \le z_{max} \end{aligned}\right\} \tag{11}$$

To account for the boundary influence of R_1 and R_2, the controlling equations are reformulated using the coordinate transformation given in [25], as $\xi = \dfrac{r - R_2}{R}$ (12)

where $R(z) = R_1(z) - R_2(z)$. Using this reform in equations (9) and (10), take the form

$$\frac{1}{(1-\phi)^{2.5}}\left[w_{\xi\xi} + \frac{R}{\xi R + R_2}w_r\right] - R^2\left(\frac{1}{D_a} + H^2\right)w + R^2G_r\Theta = R^2p_z \tag{13}$$

$$\Theta_{\xi\xi} + \frac{R}{\xi R + R_2}\Theta_{\xi} + R^2 s\,(1+3\phi) = 0 \tag{14}$$

The prescribed conditions, depicted in terms of the transformed coordinates, are as follows

$$\left.\begin{array}{llllll} w_{\xi} = 0, & \Theta_{\xi} = 0, & \text{on} & \xi = 0 & \text{for} & 0 \le z \le z_3 \\ w = 0, & \Theta = 0 & \text{on} & \xi = 1 & \text{for} & \text{all} \quad z \\ w = 0, & \Theta_{\xi} = 0 & \text{on} & \xi = 0 & \text{for} & z_3 \le z \le z_{max} \end{array}\right\} \tag{15}$$

Key observable quantities such as temperature, flow rate, impedance, and shear stress are evaluated for both the parent and daughter arteries over a range of relevant parameter values, and the results are illustrated graphically. Flow rate in the parent artery (Q_p) and daughter artery (Q_d) are determined as follows

$$Q_p = 2\pi R\left[R\int_0^1 \xi\, w\, d\xi + R_2\int_0^1 w\, d\xi\right], \quad and \quad Q_d = \pi R\left[R\int_0^1 \xi\, w\, d\xi + R_2\int_0^1 w\, d\xi\right] \tag{16}$$

To quantify the obstruction to unidirectional flow, the resistive impedance λ_p and λ_d for the parent and daughter arteries are calculated as below

$$(\lambda_p)_i = \left|\frac{z_3 p_z}{Q_p}\right| \quad for \quad z < z_3 \quad \text{and} \quad (\lambda_d)_i = \frac{(z_{max} - z_3)\,\mathrm{p}_z}{Q_d} \tag{17}$$

Both inner and outer wall shear stresses are analyzed by means of

$$\tau = \frac{\mu_f}{(1-\phi)^{2.5}}\frac{1}{R}\,w_{\xi}. \tag{18}$$

3. Numerical Solution and Results:

Equations (13) and (14), together with the conditions (15), are transformed to a block tri-diagonal system using a two-dimensional computational grid and subsequently solved via the block elimination method.

4. Discussion:

The current investigation aims to assess the significance of Darcy parameter on blood flow passing through a bifurcated artery has tiny stenosis in the parent block. For numerical analysis, $a = 5\ mm$, $d' = 10\ mm$, $l_0 = 5\ mm$, $\beta = \pi/10$, $r_1 = 0.51a$, $\varepsilon = 2a$, $H=0.4$, $s=0.2$, $\mu = 0.894$, nano particle volume fraction $\phi = 0.2$, $G_r=0.3$ and $p_z = 0.2$ have been used.

The relationship between Darcy number (Da) and flow rate is shown in fig. 2a. An enhancement in Da drives to an enhancement in flow rate of the nanofluid blood near the flow divider and inside the daughter artery. This progress in flow characteristics through improved microcirculation may control the numbness across multiple areas of the body, especially in the legs and hands.

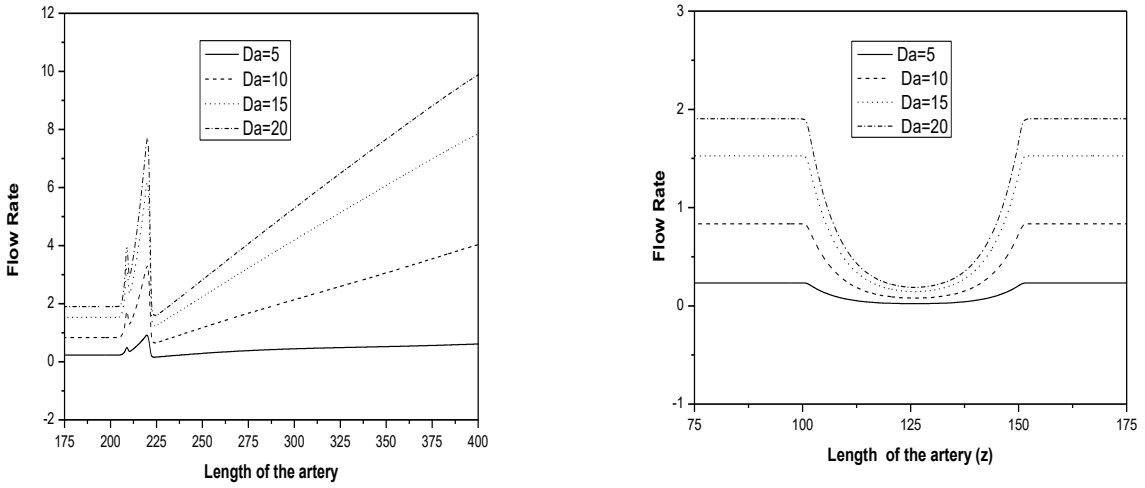

Fig. 2: Variations of flow rate with respect to the porous parameter (a) near the apex and daughter artery (b) both sides of the stenosis for other parameters.

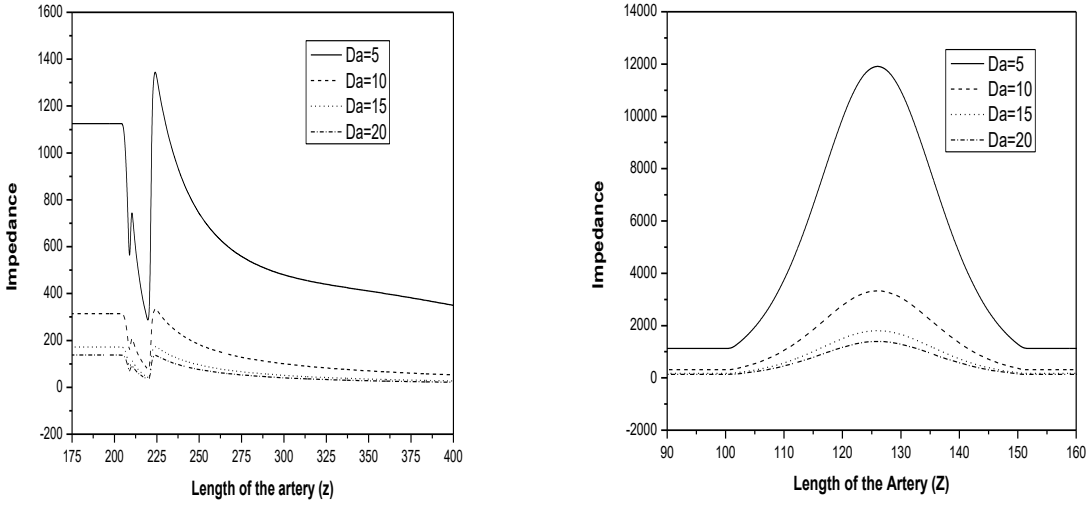

Fig. 3: Variations of impedance with respect to the porous parameter (a) near the apex and daughter artery (b) both sides of the stenosis for other parameters.

Fig. 2b shows that flow rate increases with an enhanced vales of Darcy number in the parent artery, particularly on both sides of the stenosis. Results in Fig. 3a presented that impedance diminishes with progressed vales of Darcy number in flow division region and downstream inside the daughter artery. Impedance is decreasing with enhanced vales of Darcy number which has been depicted in Fig. 3b.

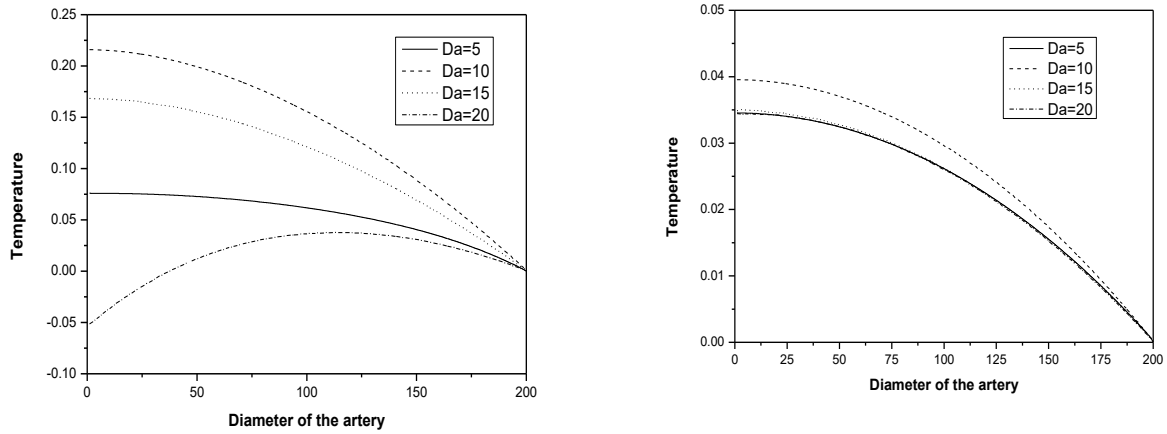

Fig. 4: Temperature gradients with respect to the porous parameter in the (a) daughter (b) parent arteries for other parameters.

Temperature gradients with respect to the porous parameter for different values have been respectively shown in fig. 4a and fig. 4b. It is understand from fig. 4a to fig. 4b that small Darcy number represents lower permeable or denser tissues, therefore there is a restriction on blood flow and convection is very weak in daughter and parent arteries.

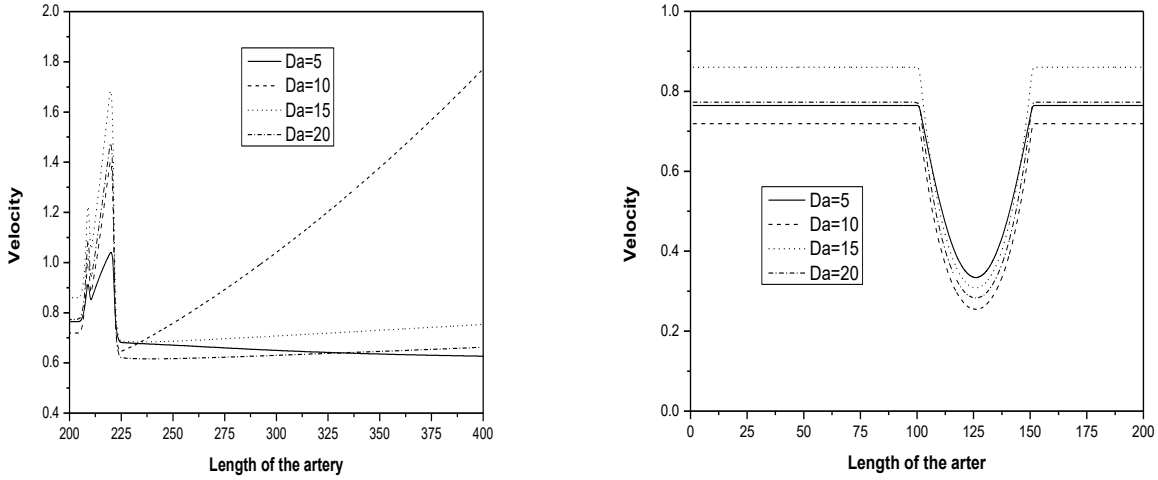

Fig. 5: Fluctuations of velocity profiles with respect to the porous parameter in the (a) daughter (b) parent arteries for other parameters.

Figs. 5a and 5b respectively represent the repercussion of Darcy number on velocity profile of nanofluid blood flow through daughter and parent arteries. From these figures, we conclude that porous medium permits effortless flow for higher Darcy number and if viscous effects dominate the flow then velocity profiles are more complex.

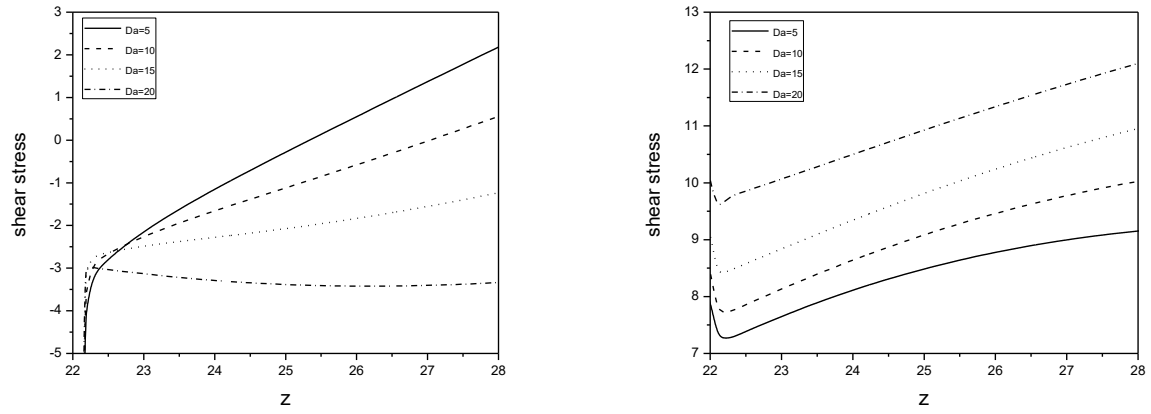

Fig. 6: Alterations of frictional stress with respect to the porous parameter through (a) inner (b) outer walls.

Fig. 6(a) shows that the shear stress decreases through the inner wall while fig. 6(b) shows that shear stress escalates through the outer wall for enhanced values of Darcy number.

5. Conclusions:

The significance of Darcy number on nanofluid blood flow through a branched artery have mild stenosis has been analyzed for the different physical magnitudes such as velocity profiles, temperature, flow rate, obstruction to the flow and shear stress. It is concluded that flow rate has been enhanced with the improved values of Darcy number while resistive impedance has been decreased. Velocity and temperature profiles have behaved for low Darcy number.

Acknowledgements: Authors are expressing heartfelt thanks to the editorial board and reviewers for their continues support.

Declaration of Interests

The authors declare that they have no known competing financial interests or personal relationships that could have appeared to influence the work reported in this paper.

CRediT authorship contribution statement

G Madhava Rao : Writing – original draft, Supervision, Investigation, Conceptualization. Funding acquisition, Formal analysis. **Adigoppula Raju:** Writing – review & editing, Supervision. **G Swamy Raddy:** review & editing, Resources, Conceptualization. Funding acquisition.

References

1. Amos, E., Omamoke, E., Nwaigwe, C. (2022). MHD pulsatile blood flow through an inclined stenosed artery with body acceleration and slip effects. *International Journal of Theoretical and Applied Mathematics*, 8(1), 1–3.
2. Bali, R., Awasthi, U. (2007). Effect of a magnetic field on the resistance to blood flow through stenotic artery. *Applied Mathematics and Computation*, 188(2), 1635–1641.
3. Berselli, L. C., Miloro, P., Menciassi, A., Sinibaldi, E. (2013). Exact solution to the inverse Womersley problem for pulsatile flows in cylindrical vessels, with application to magnetic particle targeting. *Applied Mathematics and Computation*, 219(10), 5717–5729.
4. Berselli, L. C., Guerra, F., Mazzolai, B., Sinibaldi, E. (2014). Pulsatile viscous flows in elliptical vessels and annuli: solution to the inverse problem, with application to blood and cerebrospinal fluid flow. *SIAM Journal on Applied Mathematics*, 74(1), 40–59.
5. Chakravarty, S., Mandal, P. K. (1997). An analysis of pulsatile flow in a model aortic bifurcation. *International Journal of Engineering Science*, 35(4), 409–422.
6. Dash, R. K., Mehta, K. N., Jayaraman, G. (1996). Casson fluid flow in a pipe filled with a homogeneous porous medium. *International Journal of Engineering Science*, 34(10), 1145–1156.

7. Elshehawey, E., Elbarbary, E. M., Afifi, N., El-Shahed, M. (2000). Pulsatile flow of blood through a porous medium under periodic body acceleration. *International Journal of Theoretical Physics*, 39, 183–188.
8. El-Shahed, M. (2003). Pulsatile flow of blood through a stenosed porous medium under periodic body acceleration. *Applied Mathematics and Computation*, 138(2–3), 479–488.
9. Gandhi, R., Sharma, B. K., Mishra, N. K., Al-Mdallal, Q. M. (2023). Computer simulations of EMHD Casson nanofluid flow of blood through an irregular stenotic permeable artery: application of Koo–Kleinstreuer–Li correlations. *Nanomaterials* 13(4), 652.
10. Kiran, G. R., Murthy, V. R., Radhakrishnamacharya, G. (2019). Pulsatile flow of a dusty fluid through a constricted channel in the presence of magnetic field. *Materials Today: Proceedings*, 19, 2645–2649.
11. Karim, A., Uddin, M. N., Akter, M. (2021). Geometrical analysis to blood flow across tapered–non-tapered arteries by the use of various advanced flow parameters. *Journal of Information and Mathematical Sciences*, 13(1), 2021.
12. Lindroos, M., Kupari, M., Heikkilä, J., Tilvis, R. (1993). Prevalence of aortic valve abnormalities in the elderly: An echocardiographic study of a random population sample. *Journal of the American College of Cardiology*, 21, 1220–1225.
13. Liu, Y., Liu, W. (2020). Blood flow analysis in tapered stenosed arteries with the influence of heat and mass transfer. *Journal of Applied Mathematics and Computation*, 63, 523–541.
14. Madhava Rao, G., Srinivasacharya, D., Kotireddy, N. (2019). Flow of blood through a porous bifurcated artery with mild stenosis under the influence of applied magnetic field. *Numerical Heat Transfer, Part A: Applications*, (year not provided), 233–240.

Mandal, P. K. (2005). An unsteady analysis of non-Newtonian blood flow through tapered arteries with a stenosis. *International Journal of Non-Linear Mechanics*, 40(1), 151–164.

15. Mandal, P. K., Chakravarty, S., Mandal, A., Amin, N. A. (2007). Effect of body acceleration on unsteady pulsatile flow of non-Newtonian fluid through a stenosed artery. *Applied Mathematics and Computation*, 189(1), 766–779.
16. Sarkar, A., Jayaraman, G. (1998). Correction to flow rate–pressure drop relation in coronary angioplasty: steady streaming effect. *Journal of Biomechanics*, 31(9), 781–791.
17. Shahzadi, I., Duraihem, F. Z., Ijaz, S., Raju, C., Saleem, S. (2023). Blood stream alternations by means of electroosmotic forces of fractional ternary nanofluid through the oblique stenosed aneurysmal artery with slip conditions. *International Communications in Heat and Mass Transfer*, 143, 106679.
18. Srinivasacharya, D., Madhava Rao, G. (2016). Magnetic field effects for copper suspended nanofluid venture through a bifurcated artery. *Journal of Nanofluids*, 5(5), 774–782.
19. Srinivasacharya, D., Madhava Rao, G. (2017). Modeling of blood flow through a bifurcated artery using nanofluid. *BioNanoScience*, 7(3), 464–474.
20. Stewart, B. F., Siscovick, D., Lind, B. K., Gardin, J. M., Gottdiener, J. S., Smith, V. E., Kitzman, D. W., Otto, C. M. (1997). Clinical factors associated with calcific aortic valve disease. *Journal of the American College of Cardiology*, 29, 630–634.
21. Young, D. F., Tsai, F. Y. (1973). Flow characteristics in models of arterial stenoses—I. Steady flow. *Journal of Biomechanics*, 6(4), 395–410.